Veatch, W. R., Fossel, E. T., & Blout, E. R. (1974) *Biochemistry 13*, 5249-5256.
Vega, A. J., & Luz, Z. (1987) *J. Chem. Phys. 86*, 1803-1813.
Venkatachalam, C. M., & Urry, D. W. (1983) *J. Comput. Chem. 4*, 461-469.
Wallace, B. A., Veatch, W. R., & Blout, E. R. (1981) *Biochemistry 20*, 5754-5760.
Weinstein, S., Wallace, B. A., Blout, E. R., Morrow, J. S., & Veatch, W. (1979) *Proc. Natl. Acad. Sci. U.S.A. 76*, 4230-4234.
Weinstein, S., Wallace, B. A., Morrow, J. S., & Veatch, W. R. (1980) *J. Mol. Biol. 143*, 1-19.
Weinstein, S., Durkin, J. T., Veatch, W. R., & Blout, E. R. (1985) *Biochemistry 24*, 4374-4382.

Deuterium NMR of ^{2}HCO-Val^1···Gramicidin A and ^{2}HCO-Val^1-D-Leu^2···Gramicidin A in Oriented DMPC Bilayers†

Andrew W. Hing,*,‡ Steven P. Adams,§ David F. Silbert,∥ and Richard E. Norberg‡

Department of Physics, Washington University, St. Louis, Missouri 63130, Department of Biochemistry and Molecular Biophysics, Washington University, St. Louis, Missouri 63110, and Central Research Laboratory, Monsanto Company, Chesterfield, Missouri 63198

Received June 27, 1989; Revised Manuscript Received December 8, 1989

ABSTRACT: Deuterium NMR is used to study the structure and dynamics of the formyl C–^{2}H bond in selectively deuterated gramicidin molecules. Specifically, the functionally different analogues ^{2}HCO-Val^1···gramicidin A and ^{2}HCO-Val^1-D-Leu^2···gramicidin A are studied by ^{2}H NMR so that any conformational or dynamical differences between the two analogues can be correlated with their difference in lifetime. These analogues are first synthesized, purified, and characterized and then incorporated into oriented bilayers of dimyristoylphosphatidylcholine sandwiched between glass coverslips. Phosphorus NMR line shapes obtained from these samples are consistent with the presence of the bilayer phase and indicate that the disorder exhibited by the lipid matrix is approximately of the same type and degree for both analogues. Deuterium NMR line shapes obtained from these samples indicate that the motional axis of the formyl group of gramicidin is parallel to the coverslip normal, that the distribution of motional axis orientations has a width of 7–9°, and that a similar, major conformational and dynamical state exists for the formyl C–^{2}H bond of both analogues. In this state, if the only motion present is fast axial rotation, then the experimentally derived angle between the formyl C–^{2}H bond and the motional axis is consistent with the presence of a right-handed, single-stranded, $\beta^{6.3}$ helical dimer but is not consistent with the presence of a left-handed, single-stranded, $\beta^{6.3}$ helical dimer. However, if fast axial rotation is not the only motion present, then the left-handed, single-stranded, $\beta^{6.3}$ helical dimer cannot be absolutely excluded as a possibility. Also, a second, minor conformational and dynamical state appears to be present in the spectrum of ^{2}HCO-Val^1-D-Leu^2···gramicidin A but is not observed in the spectrum of ^{2}HCO-Val^1···gramicidin A. This minor conformational and dynamical state may reflect the presence of monomers, while the major conformational and dynamical state may reflect the presence of dimers.

One of the most important properties of the linear peptide gramicidin is its ability to form ion channels in model membranes (Hladky & Haydon, 1970, 1972). Ion channels in cell membranes are extremely important for cellular functions such as controlling the internal environment, maintaining a membrane potential, and, in nerve cells, propagating an action potential. It is hoped that the study of a model ion channel such as gramicidin will lead to general insights about how ion channels work. One of the most important insights to be gained is how function is related to structure. Thus, one of the most important questions about gramicidin centers on how the functional aspects of the channel are related to the channel's three-dimensional structure in a membrane.

One of the important functional properties of the gramicidin channel is the channel's kinetics of formation and dissociation. In the process of forming an ion channel, two nonconducting monomers combine to form a conducting dimer (Hladky & Haydon, 1970, 1972; Bamberg & Läuger, 1973, 1974; Zingsheim & Neher, 1974; Kolb et al., 1975; Veatch et al., 1975):

$$G + G \underset{k_D}{\overset{k_R}{\rightleftharpoons}} G_2$$

In this dimerization reaction, k_R is the rate constant of association and k_D is the rate constant of dissociation. The dissociation constant k_D is therefore equal to the reciprocal of the mean lifetime τ^* of a channel (Bamberg & Läuger, 1973; Kolb & Bamberg, 1977):

$$k_D = 1/\tau^* \quad (1)$$

Both rate constants, though, determine the equilibrium con-

†This work was supported in part by NIH Grants GMO7200, GM30244, and GM38540, ACS Grant BC198, the Department of Physics of Washington University, and the Central Research Laboratories of Monsanto Co.

*Address correspondence to this author at the Department of Physics, Box 1105, Washington University, St. Louis, MO 63130.
‡Department of Physics, Washington University.
§Monsanto Co.
∥Department of Biochemistry and Molecular Biophysics, Washington University.

0006-2960/90/0429-4156$02.50/0

stant between conducting dimers and nonconducting monomers (Bamberg & Läuger, 1973):

$$K = k_R/k_D = [G_2]/[G]^2 \quad (2)$$

where $[G_2]$ denotes the concentration of gramicidin dimers and [G] denotes the concentration of gramicidin monomers.

An important variable that can affect the channel's kinetics of formation and dissociation is the primary structure of gramicidin. For example, a comparison of Val^1···gramicidin A and Val^1-D-Leu^2···gramicidin A shows that while the single-channel conductance remains the same for both, the lifetime of Val^1-D-Leu^2···gramicidin A (210 ms) is reduced from that of Val^1···gramicidin A (800 ms) by approximately 75% (Bradley et al., 1981; Urry et al., 1983). Therefore, the decreased lifetime of Val^1-D-Leu^2···gramicidin A can be expected to result in a decreased number of conducting dimers relative to nonconducting monomers.

The reason for the decreased lifetime of Val^1-D-Leu^2··· gramicidin A relative to that of Val^1···gramicidin A must be explained in terms of the three-dimensional structure of the gramicidin channel. Specifically, the three-dimensional structure of the main ion-transporting channel of gramicidin in membranes is postulated to be a dimer composed of two left-handed, single-stranded, $\beta^{6.3}$ helices in which the formyl protons at the amino termini of the monomers are extremely close together (Urry, 1971; Urry et al., 1971). In terms of this model, the decreased lifetime resulting from substitution of D-leucine for glycine in the second amino acid position of gramicidin can be explained by a steric effect (Bradley et al., 1981). In particular, since the second amino acid residue is positioned near the intermonomeric junction, the bulky side chain of D-leucine in the second amino acid position is expected to decrease the lifetime of the dimer by destabilizing the intermonomeric hydrogen bonds (Bradley et al., 1981).

Now, since the formyl protons are extremely close together in the $\beta^{6.3}$ helical dimer model, they occupy a position in the gramicidin molecule that may be sensitive to dimer formation, and so the structure and dynamics of the formyl protons may be affected by the substitution of D-leucine for glycine in two ways. In the first case, the nature of the intermonomeric hydrogen bonding in the dimer may be altered by the D-leucine substitution, and so the conformational and dynamical state of the formyl protons may be different for the two analogues in dimer form. In the second case, if the conformation and dynamics of the formyl protons are different in dimers as compared to monomers, then the substitution of D-leucine for glycine can be expected to increase the number of formyl protons exhibiting a conformational and dynamical state characteristic of monomers.

To investigate these questions about the structure and dynamics of the formyl protons further, deuterium NMR is used to study the structure and dynamics of selectively deuterated ^{2}HCO-Val^1···gramicidin A and ^{2}HCO-Val^1-D-Leu^2···gramicidin A incorporated into oriented DMPC[1] bilayers. The data obtained from these deuterated analogues are in the form of deuterium line shapes which are analyzed in terms of quadrupolar splitting, line width, and number. This allows conclusions to be drawn about the dynamics, the conformation, the distribution of orientations about some mean orientation, and the number of conformational and dynamical states of the formyl C–^{2}H bond on the NMR time scale. This experimental data can then be compared with theoretical predictions of structure. More importantly, the formyl groups of two functionally different gramicidin analogues are studied by deuterium NMR so that any possible structural or dynamical differences between the two analogues can be correlated with the functional difference.

Experimental Procedures

^{2}HCO-Val^1···Gramicidin A Synthesis

Synthesis. Selective deuteration of the formyl group of Val^1···gramicidin A is accomplished by first isolating the Val^1···gramicidin A component from the natural mixture by countercurrent chromatography performed on a coil planet centrifuge (P. C. Inc.) (Ito, 1986) according to the procedure outlined by Ito et al. (1982). This compound is then deformylated by reaction with hydrogen chloride in methanol, and the desformyl Val^1···gramicidin A is separated from unreacted material by ion-exchange chromatography; both of these steps are performed according to the procedure outlined by Sarges and Witkop (1965). The amino terminus of the molecule is then formylated by reaction with ^{2}HCOOH (MSD Isotopes) and acetic anhydride essentially according to the procedure described by Prasad et al. (1982).

Purification. The crude ^{2}HCO-Val^1···gramicidin A is purified according to the procedure described previously for the purification of Val^1···(2-^{2}H)Ala^3···gramicidin A (Hing et al., 1990).

Characterization. The purified ^{2}HCO-Val^1···gramicidin A is characterized by HPLC, TLC, ^{13}C NMR, mass spectrometry, and amino acid analysis.

^{2}HCO-Val^1-D-Leu^2···Gramicidin A Synthesis

Synthesis. The synthesis of ^{2}HCO-Val^1-D-Leu^2···gramicidin A is accomplished essentially according to the procedure described previously for the synthesis of Val^1···(2-^{2}H)Ala^3··· gramicidin A (Hing et al., 1990) except that the amino terminus is formylated by reaction with ^{2}HCOOH (Cambridge Isotope Laboratories) and acetic anhydride.

Purification. The crude ^{2}HCO-Val^1-D-Leu^2···gramicidin A is purified in the same way as the crude ^{2}HCO-Val^1···gramicidin A except that toluene is used in the countercurrent chromatographic solvent mixture instead of benzene.

Characterization. The purified ^{2}HCO-Val^1-D-Leu^2···gramicidin A is characterized by HPLC, TLC, ^{13}C NMR, mass spectrometry, and amino acid analysis.

Sample Preparation

Except for a few details, the incorporation of ^{2}HCO-Val^1···gramicidin A and ^{2}HCO-Val^1-D-Leu^2···gramicidin A into oriented DMPC bilayers is accomplished by the procedure outlined by Seelig et al. (1985) and Nicholson et al. (1987) with the modifications described previously (Hing et al., 1990). Those details of the sample preparation procedure that are different in this study include initial deposition of the 10:1 lipid:peptide mixture onto only one side of a coverslip and hydration and alignment of the sample for 35 h at 44–49 °C and for 39 h at 54 °C. The ^{2}HCO-Val^1···gramicidin A–DMPC sample contains approximately 53–59 mg of peptide while the ^{2}HCO-Val^1-D-Leu^2···gramicidin A–DMPC sample contains approximately 63 mg of peptide.

NMR Probe and Data Acquisition

The NMR probe and data acquisition parameters used to obtain the proton-decoupled phosphorus and deuterium spectra are the same as described before (Hing et al., 1990). As

[1] Abbreviations: DMPC, dimyristoylphosphatidylcholine; GA, gramicidin A; GB, gramicidin B; GC, gramicidin C; HPLC, high-performance liquid chromatography; TLC, thin-layer chromatography; T_2, spin–spin relaxation time; t_R, time between repetitions of pulse sequence; τ, time between pulses of quadrupole echo sequence.

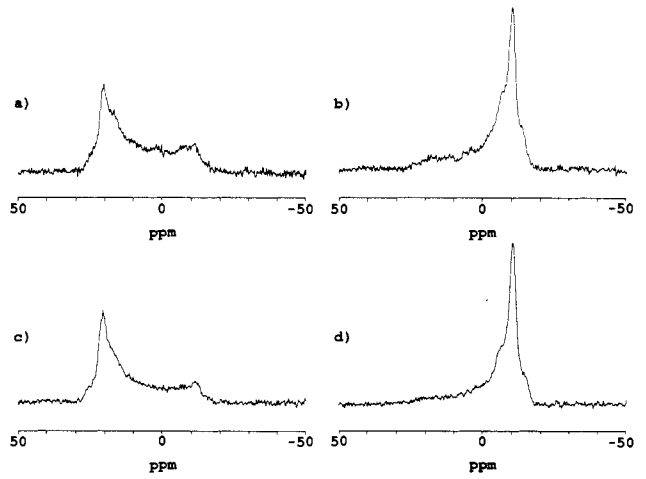

FIGURE 1: Orientation dependence of the ^{31}P NMR spectrum of DMPC bilayers containing ^{2}HCO-Val^1···gramicidin A oriented at (a) $\beta = 0°$ and (b) $\beta = 90°$ and of DMPC bilayers containing ^{2}HCO-Val^1-D-Leu^2···gramicidin A oriented at (c) $\beta = 0°$ and (d) $\beta = 90°$. All spectra are acquired at $T = 54$ °C with $t_R = 10.0$ s, 12 scans, and ^{1}H decoupling.

before, the angle between the normal to the glass coverslips and the direction of the magnetic field is designated β.

RESULTS

Phosphorus NMR

Phosphorus NMR spectra of the ^{2}HCO-Val^1···gramicidin A–DMPC sample acquired at $T = 54$ °C are shown in parts a and b of Figure 1, while phosphorus NMR spectra of the ^{2}HCO-Val^1-D-Leu^2···gramicidin A–DMPC sample acquired at $T = 54$ °C are shown in parts c and d of Figure 1. Parts a and c of Figure 1 correspond to samples oriented at $\beta = 0°$, while parts b and d of Figure 1 correspond to samples oriented at $\beta = 90°$. The temperature of the phase transition between the liquid-crystalline and gel states has been shown for similar mixtures of phosphatidylcholine and gramicidin to occur within a few degrees of the phase transition temperature of the pure lipid (Chapman et al., 1974, 1977; Nicholson et al., 1987). Consequently, the spectra of Figure 1 are obtained above the phase transition temperature.

Molecular Orientation. For both samples, the variation of the resonance frequency of the main peak with sample orientation indicates that the DMPC headgroups rotate rapidly about an axis close to parallel to the normal to the glass coverslips (Seelig, 1978).

Distribution of Orientations. For both samples, the orientation dependence of the main peak's width and symmetry can be explained to a large extent by inhomogeneous line broadening arising from DMPC headgroups not all possessing the same angle between the axis of motional averaging and the normal to the glass coverslip; most likely, a distribution of phosphocholine motional axis orientations exists in which most motional axes are aligned close to parallel to the coverslip normal. Moreover, from the line width of the resonance for $\beta = 0°$ and an assumed fixed, homogeneous line-width contribution, an estimate can be made of the width of the distribution of phosphocholine motional axis orientations. For the ^{2}HCO-Val^1···gramicidin A–DMPC sample, this width is estimated to be $\sim 20°$, and for the ^{2}HCO-Val^1-D-Leu^2··· gramicidin A–DMPC sample, this width is estimated to be $\sim 16°$. Although the line shapes of Figure 1 show that the alignment of the DMPC headgroup motional axes is not perfect, the important point to consider about this imperfect alignment is that the lipid matrix surrounding ^{2}HCO-Val^1···gramicidin A and the lipid matrix surrounding ^{2}HCO-Val^1-D-Leu^2···gramicidin A exhibit approximately the same type and degree of disorder.

Table I: ^{2}H NMR Quadrupolar Splittings and Line Widths of ^{2}HCO-Val^1···Gramicidin A in Oriented DMPC Bilayers as a Function of Temperature and Sample Orientation

	$\beta = 0°$		$\beta = 90°$	
T (°C)	$\lvert\Delta\nu_Q\rvert$[a] (Hz)	fwhm[b] (Hz)	$\lvert\Delta\nu_Q\rvert$ (Hz)	fwhm (Hz)
54	26 400	1200	13 400	2300
44	28 900	1200	N/O[c]	N/O
34	31 300	2100	N/O	N/O

[a] $\lvert\Delta\nu_Q\rvert$ is measured from the center of one resonance line to the center of the other resonance line and is resolved to 1600 Hz. [b] fwhm is the full width of the resonance line at half-intensity. [c] N/O means that the data could not be observed in the spectrum.

Table II: ^{2}H NMR Quadrupolar Splittings and Line Widths of ^{2}HCO-Val^1-D-Leu^2···Gramicidin A in Oriented DMPC Bilayers as a Function of Temperature and Sample Orientation

	$\beta = 0°$		$\beta = 90°$	
T (°C)	$\lvert\Delta\nu_Q\rvert$[a] (Hz)	fwhm[b] (Hz)	$\lvert\Delta\nu_Q\rvert$ (Hz)	fwhm (Hz)
54	24 400	1300	11 000	2300
44	26 400	1200	N/O[c]	N/O
34	29 300	1800	N/O	N/O

[a] $\lvert\Delta\nu_Q\rvert$ is measured from the center of one resonance line to the center of the other resonance line and is resolved to 1600 Hz. [b] fwhm is the full width of the resonance line at half-intensity. [c] N/O means that the data could not be observed in the spectrum.

Number of Phases. No signals are present in the spectra of Figure 1 that could be interpreted to indicate the presence of the inverted hexagonal phase or phases consisting of DMPC molecules undergoing fast isotropic motion. However, the spectra of Figure 1 do indicate that a component corresponding to a random orientation of motional axes is present in a small amount.

Deuterium NMR

Deuterium NMR spectra of ^{2}HCO-Val^1···gramicidin A incorporated into oriented bilayers of DMPC are shown in Figure 2 as a function of macroscopic sample orientation and temperature. Parts a–f of Figure 2 correspond to a sample oriented at $\beta = 0°$, while parts g–l of Figure 2 correspond to a sample oriented at $\beta = 90°$. The quadrupolar splittings and line widths of the main deuterium resonance lines of Figure 2 are listed in Table I. Deuterium NMR spectra of ^{2}HCO-Val^1-D-Leu^2···gramicidin A incorporated into oriented bilayers of DMPC are shown in Figure 3 as a function of macroscopic sample orientation and temperature. Parts a–f of Figure 3 correspond to a sample oriented at $\beta = 0°$, while parts g–l of Figure 3 correspond to a sample oriented at $\beta = 90°$. The quadrupolar splittings and line widths of the main deuterium resonance lines of Figure 3 are listed in Table II.

Effect of T_2 Relaxation on Membrane Spectra. Interpretation of the intensity and line-shape changes in the deuterium spectra yields some information about the effects of T_2 relaxation on the observed spectra. In general, the variation in intensity and line shape as a function of temperature and sample orientation exhibited by the resonance lines of ^{2}HCO-Val^1-D-Leu^2···gramicidin A (Figure 3) is the same as that exhibited by the resonance lines of ^{2}HCO-Val^1···gramicidin A (Figure 2); consequently, the interpretation of intensity and line-shape changes in terms of T_2 relaxation effects for ^{2}HCO-Val^1-D-Leu^2···gramicidin A is the same as that for ^{2}HCO-Val^1···gramicidin A.

In Figures 2 and 3, as the temperature decreases from above the phase transition temperature, the intensity of the deuterium

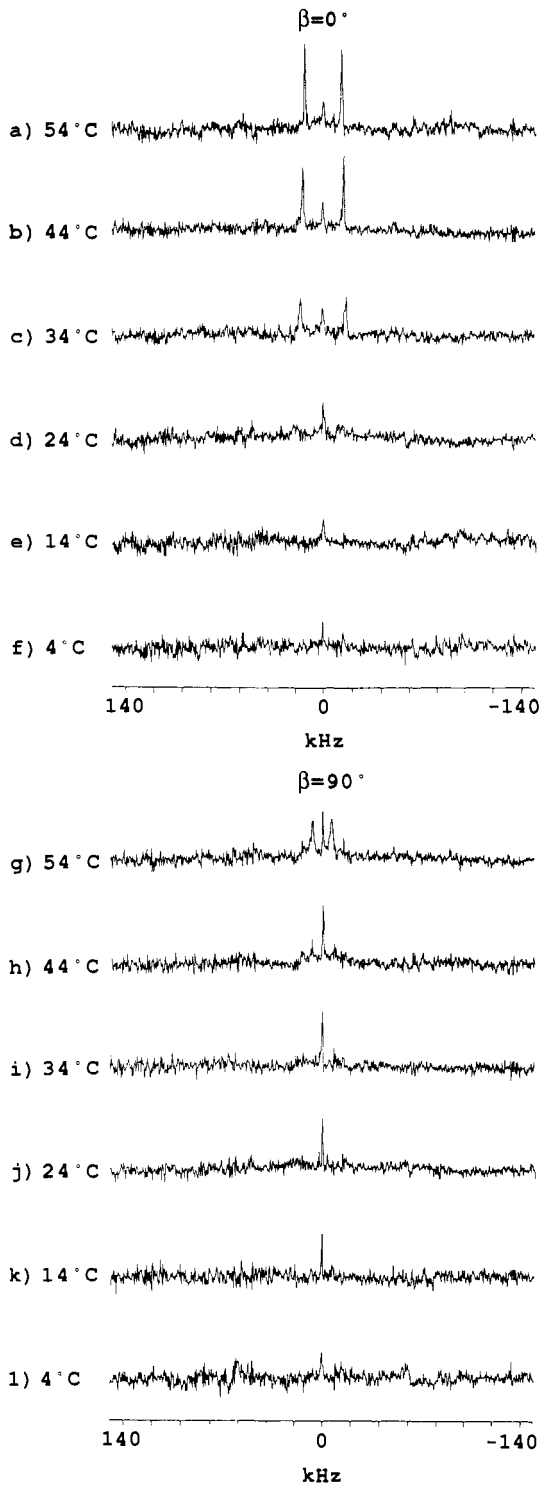

FIGURE 2: Orientation and temperature dependence of the ^{2}H NMR spectrum of ^{2}HCO-Val^1···gramicidin A in DMPC bilayers. All spectra are acquired with τ = 60 μs, t_R = 0.5 s, and ^{1}H decoupling. Spectra a–d and g–j are acquired with 120 000 scans, while spectra e, f, k, and l are acquired with 80 000 scans.

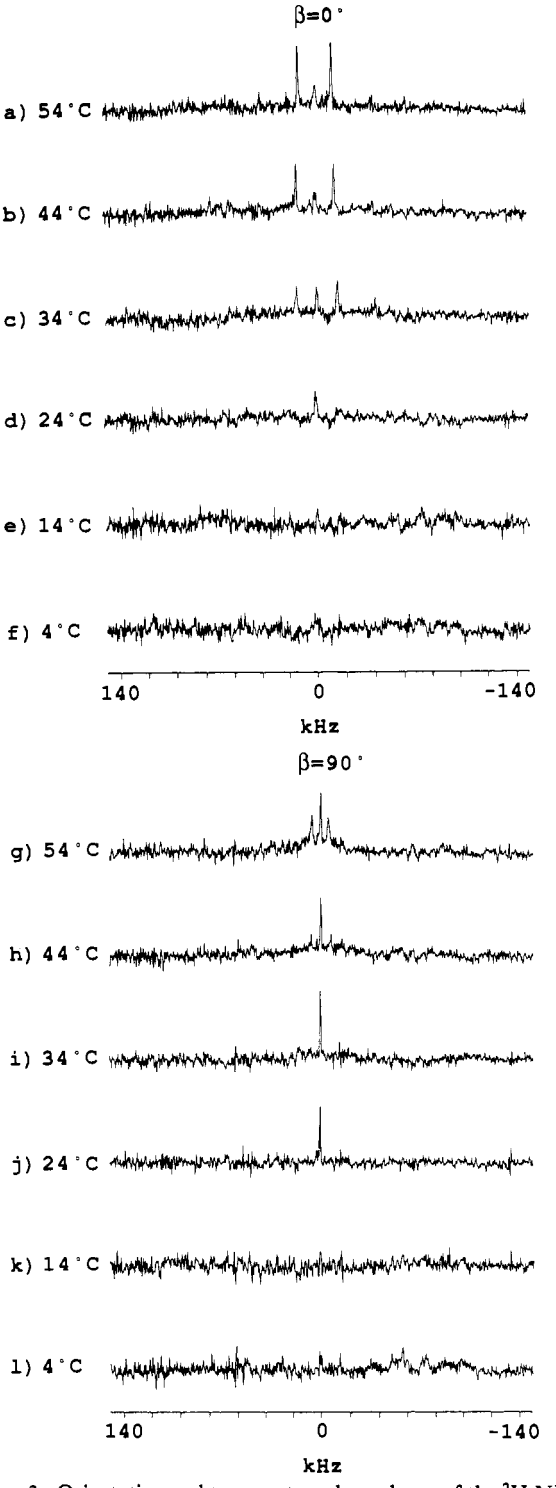

FIGURE 3: Orientation and temperature dependence of the ^{2}H NMR spectrum of ^{2}HCO-Val^1-D-Leu^2···gramicidin A in DMPC bilayers. All spectra are acquired with τ = 60 μs, t_R = 0.5 s, and ^{1}H decoupling. Spectra a–d and g–j are acquired with 120 000 scans, while spectra e, f, k, and l are acquired with 80 000 scans.

resonance lines decreases until no signal can be observed at a temperature near the phase transition temperature. As the temperature decreases below the phase transition temperature, the ^{2}H NMR signal remains small and possibly becomes noticeable only at T = 4 °C and β = 90°. The intensity decrease near the phase transition temperature can be explained by the occurrence of a minimum in the value of T_2 near the phase transition temperature which results from motion intermediate between fast axial rotation ($\gg 10^5$ Hz) and slow motion ($\ll 10^5$ Hz) (Pauls et al., 1985; Datema et al., 1986). In particular, when the temperature is near the phase transition temperature, most of the gramicidin molecules are in the intermediate motional regime, and so the ^{2}H NMR signal virtually disappears because of the small value of T_2 that most of the gramicidin molecules possess.

At temperatures above the phase transition temperature, the intensity and line width of the main deuterium resonance lines exhibit a clear dependence on sample orientation. Specifically, the intensities of the main deuterium resonance lines for the β = 90° sample orientation are decreased relative to the intensities observed for the β = 0° sample orientation.

Also, the resonance lines for the $\beta = 90°$ sample orientation appear to sit on a small, broadened hump which is not present in the spectrum corresponding to the $\beta = 0°$ sample orientation. Furthermore, as the temperature decreases, this dependence of the line intensity on sample orientation is accentuated; in other words, the distinct resonance lines observed for the $\beta = 90°$ sample orientation at $T = 54$ °C have virtually disappeared at $T = 44$ and 34 °C, while the distinct resonance lines observed for the $\beta = 0°$ sample orientation at $T = 54$ °C can still be observed at $T = 44$ and 34 °C. Also, for those deuterium nuclei yielding distinct resonance lines for both $\beta = 0°$ and $\beta = 90°$ ($T = 54$ °C), the resonance line widths show a dependence on macroscopic sample orientation (Tables I and II); in this case, the full width at half-intensity of an individual resonance line increases by approximately 1 kHz when the sample orientation is changed from $\beta = 0°$ to $\beta = 90°$.

The observed orientation dependence of the intensity and width of the deuterium resonance lines can be explained by an anisotropic T_2 relaxation mechanism. In this mechanism, $1/T_2(\beta = 90°) > 1/T_2(\beta = 0°)$ for that fraction of the deuterium nuclei exhibiting distinct resonance lines for $\beta = 90°$, $1/T_2(\beta = 90°) \gg 1/T_2(\beta = 0°)$ for that fraction of the deuterium nuclei exhibiting a broadened hump for $\beta = 90°$, and the difference between $1/T_2(\beta = 90°)$ and $1/T_2(\beta = 0°)$ increases as the temperature decreases. Changes in line shape resulting from anisotropic T_2 relaxation have been the subject of several investigations and are generally due to modulation of the quadrupolar interaction by motions occurring at intermediate rates (Pschorn & Spiess, 1980; Spiess & Sillescu, 1981; Beshah et al., 1987; Wittebort et al., 1987; Vega & Luz, 1987; Poupko et al., 1987). In the case of the oriented samples observed in Figures 2 and 3, a possible reason for T_2 to be orientation dependent is that since the axis of motional averaging for the formyl group of ^{2}HCO-Val^1···gramicidin A and ^{2}HCO-Val^1-D-Leu^2···gramicidin A is parallel to the coverslip normal, rotations about this axis for the $\beta = 0°$ sample orientation do not significantly alter the orientation of the C–^{2}H bond relative to the magnetic field and so are less effective in modulating the quadrupolar interaction and causing a decrease in the value of T_2. However, rotations about an axis parallel to the coverslip normal for $\beta = 90°$ do significantly change the orientation of the C–^{2}H bond relative to the magnetic field (unless the C–^{2}H bond is aligned parallel to the axis of motional averaging) and so are more effective in modulating the quadrupolar interaction and causing a decrease in the value of T_2. Furthermore, when decreasing temperature causes the rate of axial rotation to decrease, the modulation of the quadrupolar interaction that occurs in the $\beta = 90°$ sample orientation becomes even more effective in decreasing T_2.

Molecular Conformation. In the liquid-crystalline phase, rapid rotation of the C–^{2}H bond about an axis motionally averages the quadrupolar splitting $\Delta\nu_Q$ of the deuterium nucleus to (Seelig, 1977)

$$\Delta\nu_Q = (3/2)(e^2qQ/h)\langle(3\cos^2\theta - 1)/2\rangle(3\cos^2\beta' - 1)/2 \quad (3)$$

where e^2qQ/h is the static quadrupolar coupling constant and $(3/2)(e^2qQ/h) \approx 250$ kHz for a completely static, formyl C–^{2}H bond (Adriaenssens & Bjorkstam, 1972; Kukolich, 1969; Thadeus et al., 1964; Flygare, 1964); θ is the angle between the axis of motional averaging and the C–^{2}H bond; $\langle\ \rangle$ denotes a time average over motions occurring during the time scale of the NMR measurement; and β' is the angle between the axis of motional averaging and the direction of the magnetic field. The assumptions underlying the use of eq 3 have been stated before (Hing et al., 1990).

At $T = 54$ °C, for those deuterium nuclei that can be observed, the quadrupolar splitting varies with sample orientation in such a way that the quadrupolar splitting measured at $\beta = 0°$ is approximately twice the magnitude of the quadrupolar splitting measured at $\beta = 90°$ for both ^{2}HCO-Val^1···gramicidin A and ^{2}HCO-Val^1-D-Leu^2···gramicidin A (Tables I and II). According to eq 3, this result and the reduced magnitude of $\Delta\nu_Q$ indicate that the formyl group of ^{2}HCO-Val^1···gramicidin A and the formyl group of ^{2}HCO-Val^1-D-Leu^2···gramicidin A rotate rapidly about an axis parallel to the normal to the glass coverslips ($\beta' = \beta$).

Equation 3 also shows that the sign of $\Delta\nu_Q$ cannot be deduced for the values listed in Tables I and II because the absolute value of $\langle(3\cos^2\theta - 1)/2\rangle$ must be less than $1/2$ to produce the measured absolute values of $\Delta\nu_Q$ given that $(3/2)\cdot(e^2qQ/h) \approx 250$ kHz, and thus $\langle(3\cos^2\theta - 1)/2\rangle$ can be positive or negative.

At temperatures above the phase transition temperature, the magnitude of the quadrupolar splitting of the observable C–^{2}H bonds for the $\beta = 0°$ sample orientation is reduced relative to that expected for a completely static C–^{2}H bond and increases with decreasing temperature. If the only motion that occurs is fast rotation about a given axis, then the angle θ between the C–^{2}H bond and the motional axis can be deduced from the reduced magnitude of $\Delta\nu_Q$ through the use of eq 3. Given a value of 250 kHz for $(3/2)(e^2qQ/h)$ and the measured values of $|\Delta\nu_Q|$ for $\beta = 0°$, eq 3 yields for both analogues a value of $\theta = 51°$ at $T = 54$ °C and a value of $\theta = 50°$ at $T = 34$ °C if $\Delta\nu_Q$ is positive and a value of $\theta = 59°$ at $T = 54$ °C and a value of $\theta = 60°$ at $T = 34$ °C if $\Delta\nu_Q$ is negative. Even if $(3/2)(e^2qQ/h) = 200$ or 300 kHz, the values obtained for θ are not significantly altered. Potential reasons for the variation of $\Delta\nu_Q$ with temperature have been mentioned before (Hing et al., 1990).

The magnitudes of the quadrupolar splittings measured for ^{2}HCO-Val^1-D-Leu^2···gramicidin A (Table II) are slightly smaller than the magnitudes of the quadrupolar splittings measured for ^{2}HCO-Val^1···gramicidin A (Table I); consequently, under the assumption that fast axial rotation is the only motion present, the values of θ calculated for the formyl C–^{2}H bond of ^{2}HCO-Val^1-D-Leu^2···gramicidin A are slightly closer to an angle of $\theta = 54.7°$ than are the values of θ calculated for the formyl C–^{2}H bond of ^{2}HCO-Val^1···gramicidin A. However, the difference in θ between the two analogues is negligible at a resolution of 1°. If, however, axial rotation is not the only motion present, then the difference in quadrupolar splitting between the two analogues may not reflect a difference in θ between the two analogues but rather a dynamical difference between the two analogues. Possibly, the ^{2}HCO-Val^1-D-Leu^2···gramicidin A analogue experiences more small-amplitude, high-frequency motions at the formyl group position or more fluctuations in the orientation of the motional axis than does the ^{2}HCO-Val^1···gramicidin A analogue.

Distribution of Orientations. The line widths measured for ^{2}HCO-Val^1-D-Leu^2···gramicidin A for the $\beta = 0°$ sample orientation (Table II) are generally the same as those measured for ^{2}HCO-Val^1···gramicidin A for the $\beta = 0°$ sample orientation (Table I) in terms of value and temperature dependence. Consequently, ^{2}HCO-Val^1-D-Leu^2···gramicidin A and ^{2}HCO-Val^1···gramicidin A exhibit similar distributions of formyl C–^{2}H bond orientations about some mean orientation. The most significant orientational distribution to consider arises from C–^{2}H bonds in the formyl group of gramicidin not all

possessing the same motional axis orientation relative to the coverslip normal (Hing et al., 1990). Most likely, a distribution of motional axis orientations exists in which most motional axes are aligned parallel to the coverslip normal. Furthermore, eq 3 can be used to estimate the width of the distribution of motional axis orientations (β' angles) from the line width of the resonance. If this estimate is based on the half-width at half-intensity of the resonance line for $\beta = 0°$, then the distribution of β' angles for the formyl C–^{2}H bond in the ^{2}HCO-Val^1···gramicidin A–DMPC sample has a width of approximately 7–9°, and the distribution of β' angles for the formyl C–^{2}H bond in the ^{2}HCO-Val^1-D-Leu^2···gramicidin A–DMPC sample has a width of approximately 7–8°. The width of the distribution of motional axis orientations for ^{2}HCO-Val^1···gramicidin A is therefore approximately the same as that for ^{2}HCO-Val^1-D-Leu^2···gramicidin A.

Number of Conformational and Dynamical States. The fact that only one quadrupolar splitting of appreciable intensity is apparent in the NMR spectra of Figures 2 and 3 indicates that only one major conformational and dynamical state is likely to exist for those formyl C–^{2}H bonds that can be observed.

A component corresponding to a random orientation of the motional axes of the formyl C–^{2}H bond is not definitely observed in the spectra of Figures 2 and 3, but this may be because such a component remains buried in the noise of the spectra.

Each of the spectra in Figures 2 and 3 does definitely exhibit, though, a peak located at the center of the spectrum. As previously discussed (Hing et al., 1990), this center peak most likely arises from deuterium in water, even though deuterium-depleted water is used in most of the sample preparation steps.

In any case, no signals are observed in the spectra of Figure 2 that can definitely be said to represent the existence of other conformational and dynamical states of the formyl C–^{2}H bond in ^{2}HCO-Val^1···gramicidin A besides the major one. Other, minor conformational and dynamical states of the formyl C–^{2}H bond may actually exist, but their population or NMR relaxation characteristics must prevent the corresponding ^{2}H NMR signals from becoming visible above the spectral noise. To investigate this question further, the spectra of Figure 2a,b are added to improve the signal to noise ratio. The spectral sum that results is shown in Figure 4a. Even though the component spectra are obtained at different temperatures, any resonance lines that remain the same at $T = 54$ and 44 °C should add in a coherent fashion. Examination of the spectrum in Figure 4a shows that no other conformational and dynamical states besides the major one are readily apparent.

The spectra of Figure 3 obtained above the phase transition temperature for $\beta = 0°$, however, exhibit a number of spikes that might be interpreted to indicate the existence of other conformational and dynamical states of the formyl C–^{2}H bond of ^{2}HCO-Val^1-D-Leu^2···gramicidin A. To investigate this question further, the spectra of Figure 3a,b are added to improve the signal to noise ratio. The spectral sum that results is shown in Figure 4b. Examination of the spectrum in Figure 4b shows that two peaks are observed which can be interpreted to indicate the presence of a second, minor quadrupolar splitting whose magnitude is approximately 80 600 Hz. Although the signal to noise ratio of these peaks is not large, their exactly symmetrical positions about the center of this unsymmetrized spectrum argue that these peaks do not represent noise or artifact (only the main deuterium resonance lines are also observed to possess such symmetry). These peaks are not

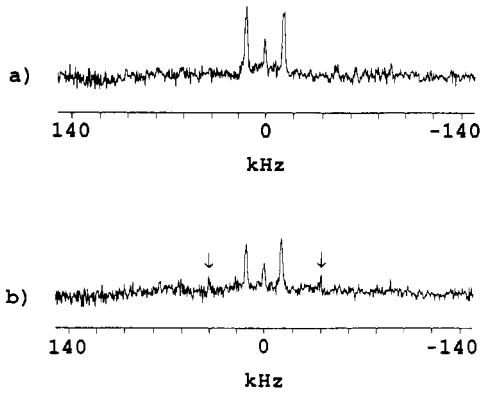

FIGURE 4: (a) ^{2}H NMR spectrum of ^{2}HCO-Val^1···gramicidin A in DMPC bilayers oriented at $\beta = 0°$ obtained by adding the spectrum corresponding to $T = 54$ °C (Figure 2a) to the spectrum corresponding to $T = 44$ °C (Figure 2b). (b) ^{2}H NMR spectrum of ^{2}HCO-Val^1-D-Leu^2···gramicidin A in DMPC bilayers oriented at $\beta = 0°$ obtained by adding the spectrum corresponding to $T = 54$ °C (Figure 3a) to the spectrum corresponding to $T = 44$ °C (Figure 3b). The arrows indicate the peaks described in the text which are located 40 300 Hz from the center of the spectrum and which are present in the spectrum of ^{2}HCO-Val^1-D-Leu^2···gramicidin A but not in the spectrum of ^{2}HCO-Val^1···gramicidin A.

apparent in the corresponding spectrum of ^{2}HCO-Val^1··· gramicidin A (Figure 4a). If fast axial rotation is the only motion present, then the quadrupolar splitting of $|\Delta\nu_Q| = 80\,600$ Hz yields a value of $\theta = 42°$ if $\Delta\nu_Q$ is positive and a value of $\theta = 70°$ if $\Delta\nu_Q$ is negative given that $(^3/_2)(e^2qQ/h) = 250$ kHz. If other, minor conformational and dynamical states of the formyl C–^{2}H bond of ^{2}HCO-Val^1-D-Leu^2··· gramicidin A exist, they are not clearly visible above the spectral noise.

Discussion

Peptide Synthesis

Characterization of the final ^{2}HCO-Val^1···gramicidin A product and the final ^{2}HCO-Val^1-D-Leu^2···gramicidin A product is especially important for the experiments described in this paper. This is because verification of the identity and purity of the final products makes unlikely the possibility that any ^{2}H NMR spectral differences between ^{2}HCO-Val^1··· gramicidin A and ^{2}HCO-Val^1-D-Leu^2···gramicidin A are due to impurities.

Sample Preparation

Since the sample preparation conditions are the same as those used before, the factors that influence the probability of obtaining the channel conformation are also the same (Hing et al., 1990). In particular, the sample preparation conditions are chosen so as to give a high probability of obtaining the channel conformation, but the definitive experiment that demonstrates the presence of a functioning channel in the unmodified solid-state NMR sample has yet to be performed.

Molecular Conformation

In general, the ^{31}P NMR spectra are consistent with the presence of a bilayer phase in which the long axes of the lipid molecules are arranged parallel to the coverslip normal. Similarly, the ^{2}H NMR spectra are consistent with an arrangement in which the long axes of the gramicidin helices are parallel to the coverslip normal, if gramicidin adopts a helical structure in the membrane and axial rotation occurs about the helical axis. This is consistent with the current picture of how gramicidin intercalates into the lipid bilayer.

Furthermore, the assumption that gramicidin forms a helical structure and rotates about the helical axis in the bilayer allows

the angle θ between the formyl C–^{2}H bond and the motional axis to be interpreted as the angle between the C–^{2}H bond and the helical axis. If fast axial rotation is assumed to be the only motion that occurs, then the angle between the formyl C–^{2}H bond and the helical axis in the liquid-crystalline phase is either 50–51 or 59–60° for the major conformational and dynamical state of both ^{2}HCO-Val^1···gramicidin A and ^{2}HCO-Val^1-D-Leu^2···gramicidin A. Therefore, the replacement of glycine with the bulkier D-leucine in the second amino acid position does not result in significant structural perturbations of the formyl group in the major conformational and dynamical state of these analogues.

In terms of the various theoretical models proposed for gramicidin structure, two factors argue against double-stranded, helical dimers as potential structural models for the major conformational and dynamical state of the gramicidin analogues studied in this paper. The double-stranded, helical dimers considered are the left-handed, antiparallel, $\beta\beta^{5.6}$ helical dimer (species 3); the right-handed, parallel, $\beta\beta^{5.6}$ helical dimer (species 4); the left-handed, parallel, $\beta\beta^{5.6}$ helical dimer that is the mirror image of species 4 (species 1); and the right-handed, antiparallel, $\beta\beta^{7.2}$ helical dimer (Veatch et al., 1974; Prasad & Chandrasekaran, 1977; Colonna-Cesari et al., 1977; Arseniev et al., 1984, 1985a; Bystrov & Arseniev, 1988). The first factor arguing against these double-stranded, helical dimers as potential structural models for the major state of the gramicidin analogues studied in this paper is that the ^{2}HCO-Val^1···gramicidin A–DMPC sample and the ^{2}HCO-Val^1-D-Leu^2···gramicidin A–DMPC sample are prepared in the same manner as the Val^1···(2-^{2}H)Ala^3···gramicidin A–DMPC sample studied earlier (Hing et al., 1990). In the latter system, the bond angle measured for the Ala^3 C_α–^{2}H bond relative to the helical axis made the double-stranded, helical dimers very unlikely candidates for structural models of gramicidin in that system. If the likely assumption is made that ^{2}HCO-Val^1···gramicidin A and ^{2}HCO-Val^1-D-Leu^2···gramicidin A in their major state in DMPC adopt the same overall structure as Val^1···(2-^{2}H)Ala^3···gramicidin A in DMPC, then double-stranded, helical dimers are also very unlikely candidates for structural models of the major conformational and dynamical state of gramicidin in the systems studied in this paper. The second factor arguing against the double-stranded, helical dimers as potential models of gramicidin structure for the major state of the analogues studied in this paper is that preliminary calculations of the formyl C–^{2}H bond angle relative to the helical axis in the double-stranded, helical dimer models yield bond angles corresponding to quadrupolar splittings $> \sim 75$ kHz in magnitude for $\beta = 0°$. Such quadrupolar splittings are not observed for the major conformational and dynamical state of gramicidin in the systems studied here; however, this last observation does not absolutely exclude double-stranded, helical dimers as potential gramicidin structures because the observed quadrupolar splittings may represent larger quadrupolar splittings that have been partially averaged by motions other than fast axial rotation. In any case, the previous statements argue that double-stranded, helical dimer models are very unlikely to represent the structure of the major conformational and dynamical state of the analogues studied in this paper.

In terms of the single-stranded, $\beta^{6.3}$ helical dimer models (Urry, 1971; Urry et al., 1971; Arseniev, 1985b), preliminary calculations show that in the left-handed model the formyl C–^{2}H bond makes an angle of $\approx$77–80° with the helical axis, while in the right-handed model the formyl C–^{2}H bond makes an angle of $\approx$58–60° with the helical axis (Venkatachalam & Urry, 1983). Therefore, the experimental, formyl C–^{2}H bond angle derived from the major quadrupolar splitting of both analogues is not consistent with the left-handed, single-stranded, $\beta^{6.3}$ helical dimer model but is consistent with the right-handed, single-stranded, $\beta^{6.3}$ helical dimer model under the assumption that fast axial rotation is the only motion present. However, the experimental data do not absolutely exclude the left-handed, single-stranded, $\beta^{6.3}$ helical dimer as a potential structure for the major conformational and dynamical state of the analogues studied in this paper because the assumption that fast axial rotation is the only motion present may not be valid. In the case that molecular motions other than fast axial rotation are present, the possibility exists that gramicidin adopts a left-handed, single-stranded, $\beta^{6.3}$ helical dimer structure in the bilayer but that quadrupolar splittings expected of formyl C–^{2}H bond angles in a rigid, axially rotating, left-handed, helical dimer ($\Delta\nu_Q \approx -106$ to -114 kHz for $\beta = 0°$) are collapsed by molecular motion other than fast axial rotation to quadrupolar splittings expected of formyl C–^{2}H bond angles in a rigid, axially rotating, right-handed, helical dimer ($\Delta\nu_Q \approx -20$ to -31 kHz for $\beta = 0°$). In this case, a calculation of θ based on the observed quadrupolar splitting, eq 3, and the assumption that fast axial rotation is the only motion present leads incorrectly to the conclusion that the right-handed, helical dimer is present. Rather, more complicated motional models must be invoked to describe the situation, and in fact, the existence of structural fluctuations in the head-to-head junction has been previously postulated to explain some functional aspects of the gramicidin channel (Heinemann et al., 1989). In any case, the experimental data derived from the major quadrupolar splitting are consistent with the right-handed, single-stranded, $\beta^{6.3}$ helical dimer model and not the left-handed model only if molecular motions other than fast axial rotation are insignificant enough that quadrupolar splittings are not collapsed by $\approx$70–90 kHz; otherwise, the left-handed model is still consistent with the experimental data. Relaxation experiments may help determine whether motions other than fast axial rotation are present to a significant extent.

Distribution of Orientations

In general, both the phosphorus and deuterium line widths can be interpreted to a large extent in terms of inhomogeneous line broadening due to a distribution of motional axis orientations in which most motional axes are aligned along the coverslip normal. For both ^{2}HCO-Val^1···gramicidin A and ^{2}HCO-Val^1-D-Leu^2···gramicidin A, the width of the distribution of phosphocholine motional axis orientations in the surrounding lipid matrix is estimated to be $\sim$16–20° in the liquid-crystalline phase, while the width of the distribution of formyl group motional axis orientations in the major conformational and dynamical state of these gramicidin analogues is estimated to be 7–9° in the liquid-crystalline phase. That the DMPC headgroup is estimated to have a wider range of motional axis orientations than the gramicidin formyl group implies either that the gramicidin helices are more ordered in the bilayer than are the phospholipid headgroups or that the estimate of the distributional width of motional axis orientations for the DMPC headgroup is not as accurate as that for the formyl C–^{2}H bond.

Number of Conformational and Dynamical States

The observation of a quadrupolar splitting ($|\Delta\nu_Q| = 80\,600$ Hz) of minor intensity in the spectrum of ^{2}HCO-Val^1-D-Leu^2···gramicidin A (Figure 4b) but not in the spectrum of ^{2}HCO-Val^1···gramicidin A (Figure 4a) can be explained in

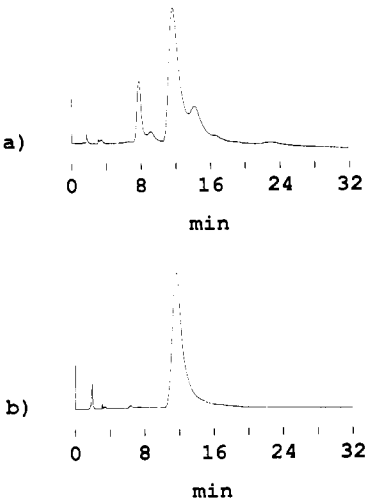

FIGURE 5: HPLC profile of (a) natural gramicidin and (b) ^{2}HCO-Val^1···gramicidin A eluted isocratically from a Vydac C_4 column at 1 mL/min with 63.5% methanol in water and detected at 214 nm with a sensitivity of 0.1 aufs. The sample is dissolved in methanol at a concentration of 1 μg/μL and injected into the column in a volume of 2 μL.

several ways. The first explanation to consider is that the minor quadrupolar splitting in the spectrum of ^{2}HCO-Val^1-D-Leu^2···gramicidin A represents an impurity generated during the synthesis of ^{2}HCO-Val^1-D-Leu^2···gramicidin A; however, the data showing the chemical characterization of ^{2}HCO-Val^1-D-Leu^2···gramicidin A (Appendix) argue that an impurity is not present in the sample in a quantity sufficient to be observable by ^{2}H NMR.

A second possible explanation to consider is that the minor quadrupolar splitting in the spectrum of ^{2}HCO-Val^1-D-Leu^2···gramicidin A reflects the existence of a minor conducting state (Busath & Szabo, 1981). However, the probability of this explanation being correct is lessened by the fact that the distribution of minor conducting states observed for ^{2}HCO-Val^1-D-Leu^2···gramicidin A is approximately the same as or even very slightly narrower than the distribution observed for ^{2}HCO-Val^1···gramicidin A (Bradley et al., 1981; Urry et al., 1983).

A third possible explanation for the presence of a minor quadrupolar splitting in the spectrum of ^{2}HCO-Val^1-D-Leu^2···gramicidin A but not in the spectrum of ^{2}HCO-Val^1···gramicidin A is that the minor quadrupolar splitting reflects ^{2}HCO-Val^1-D-Leu^2···gramicidin A molecules that have been incorporated into DMPC as nonchannel structures because ^{2}HCO-Val^1-D-Leu^2···gramicidin A does not incorporate into DMPC as the channel structure to the same degree that ^{2}HCO-Val^1···gramicidin A does. Some factors that militate against this explanation are the fact that both analogues are incorporated into DMPC under the same conditions and the fact that the lipid matrix exhibits the same behavior for both analogues as gauged by the phosphorus NMR spectra.

A last possible explanation for the presence of a minor quadrupolar splitting in the spectrum of ^{2}HCO-Val^1-D-Leu^2···gramicidin A but not in the spectrum of ^{2}HCO-Val^1···gramicidin A is that the minor quadrupolar splitting represents a structural correlate of the functional difference between the two analogues. In particular, the functional difference between the two analogues is expected to result in an altered monomer–dimer equilibrium in which the relative population of monomers is greater for ^{2}HCO-Val^1-D-Leu^2···gramicidin A than for ^{2}HCO-Val^1···gramicidin A. Therefore, the second, minor quadrupolar splitting of ^{2}HCO-Val^1-D-Leu^2···gramicidin A may represent monomers while the major quadrupolar splitting may represent dimers. The ^{2}HCO-Val^1···gramicidin A analogue does not exhibit a second, minor quadrupolar splitting possibly because these molecules exist mainly as dimers.

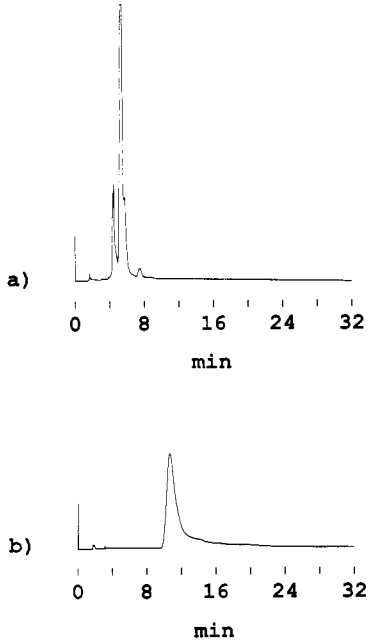

FIGURE 6: HPLC profile of (a) natural gramicidin and (b) ^{2}HCO-Val^1-D-Leu^2···gramicidin A eluted isocratically from a Vydac C_4 column at 1 mL/min with 68.5% methanol in water and detected at 214 nm with a sensitivity of 0.1 aufs. The sample is dissolved in methanol at a concentration of 1 μg/μL and injected into the column in a volume of (a) 1 and (b) 2 μL.

Table III: Amino Acid Analysis[a] of Natural Gramicidin, ^{2}HCO-Val^1···Gramicidin A, and ^{2}HCO-Val^1-D-Leu^2···Gramicidin A

	natural gramicidin		^{2}HCO-Val^1··· GA		^{2}HCO-Val^1-D-Leu^2···GA	
amino acid	expt	theory	expt	theory	expt	theory
glycine	1.05	1.00	1.07	1.00	0.00	0.00
alanine	2.06	2.00	2.02	2.00	2.02	2.00
valine	3.67	3.86[b]	3.88	4.00	3.73	4.00
isoleucine	0.08	0.14[b]	0.00	0.00	0.00	0.00
leucine	4.00	4.00	4.00	4.00	5.00	5.00
tyrosine	0.23	0.19[c]	0.00	0.00	0.00	0.00
phenylalanine	0.00	0.09[c]	0.00	0.00	0.00	0.00

[a] Hydrolysis is performed for 4 h at 145 °C in hydrochloric acid/propionic acid with 0.1% phenol; hydrolysate is redissolved in a 0.2 M sodium citrate buffer of pH 2.2, injected onto a Beckman Model 6300 amino acid analyzer that resolves amino acids by ion exchange, eluted according to the manufacturer's protocols, and detected by a postcolumn ninhydrin method at 440 and 570 nm. [b] Based on amounts of Val^1···GA, Ile^1···GA, Val^1···GC, and Ile^1···GC obtained from natural gramicidin by countercurrent chromatography performed on a coil planet centrifuge. [c] Based on a ratio of 72:9:19 for GA:GB:GC (Glickson et al., 1972).

Appendix: Peptide Characterization

Characterization of the final ^{2}HCO-Val^1···gramicidin A product and final ^{2}HCO-Val^1-D-Leu^2···gramicidin A product by HPLC, TLC, ^{13}C NMR, mass spectrometry, and amino acid analysis results in the data shown in Figures 5–9 and Table III. In general, characterization of the final products by the aforementioned techniques results in confirmation of the identity and purity of the products.

Characterization of the ^{2}HCO-Val^1···gramicidin A product by HPLC results in the chromatograms shown in Figure 5. Figure 5a is the chromatogram of natural gramicidin (ICN) and shows that the components of natural gramicidin can be

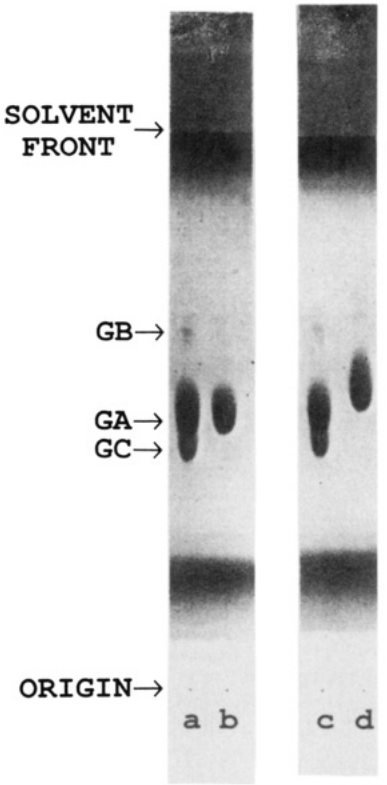

FIGURE 7: TLC deposition of (a, c) natural gramicidin, (b) ^{2}HCO-Val^1···gramicidin A, and (d) ^{2}HCO-Val^1-D-Leu^2···gramicidin A onto a Whatman LK5, silica gel 80-Å, 250-μm TLC plate. The sample is dissolved in methanol at a concentration of 6 μg/μL, deposited onto the plate in a volume of 2 μL, developed with chloroform/methanol/acetic acid (85:15:3), and visualized by exposure to iodine vapors.

identified under these HPLC conditions (Urry et al., 1983). Figure 5b is the chromatogram of synthetic ^{2}HCO-Val^1··· gramicidin A and indicates that the synthetic gramicidin possesses the same retention time as the corresponding natural Val^1···gramicidin A component and that the synthetic product is pure.

Characterization of the ^{2}HCO-Val^1-D-Leu^2···gramicidin A product by HPLC results in the chromatograms shown in Figure 6. This product is eluted with a solvent slightly more concentrated in methanol than that used to elute ^{2}HCO-Val^1···gramicidin A because of the more hydrophobic nature of ^{2}HCO-Val^1-D-Leu^2···gramicidin A. Figure 6a shows how natural gramicidin elutes under these HPLC conditions. Figure 6b shows that ^{2}HCO-Val^1-D-Leu^2···gramicidin A elutes after the major components of natural gramicidin and that the synthetic product is pure. A more pronounced tailing of the HPLC peak of ^{2}HCO-Val^1-D-Leu^2···gramicidin A is observed probably because this product's greater hydrophobicity results in a stronger interaction with the reversed-phase column.

Analytical TLC performed on the final products results in the thin-layer chromatograms shown in Figure 7. In columns a and c, the major components of natural gramicidin deposit onto the TLC plate in the same order as they elute from the HPLC column. In column b, the ^{2}HCO-Val^1···gramicidin A product is shown to deposit onto the TLC plate with the same R_f value as its natural counterpart. Also, the existence of only one TLC spot for this synthetic gramicidin indicates that this product is pure. In column d, the ^{2}HCO-Val^1-D-Leu^2···gramicidin A product deposits onto the TLC plate after the gramicidin A and C components of natural gramicidin have deposited, and the existence of one major TLC spot for this synthetic gramicidin indicates that this product is pure.

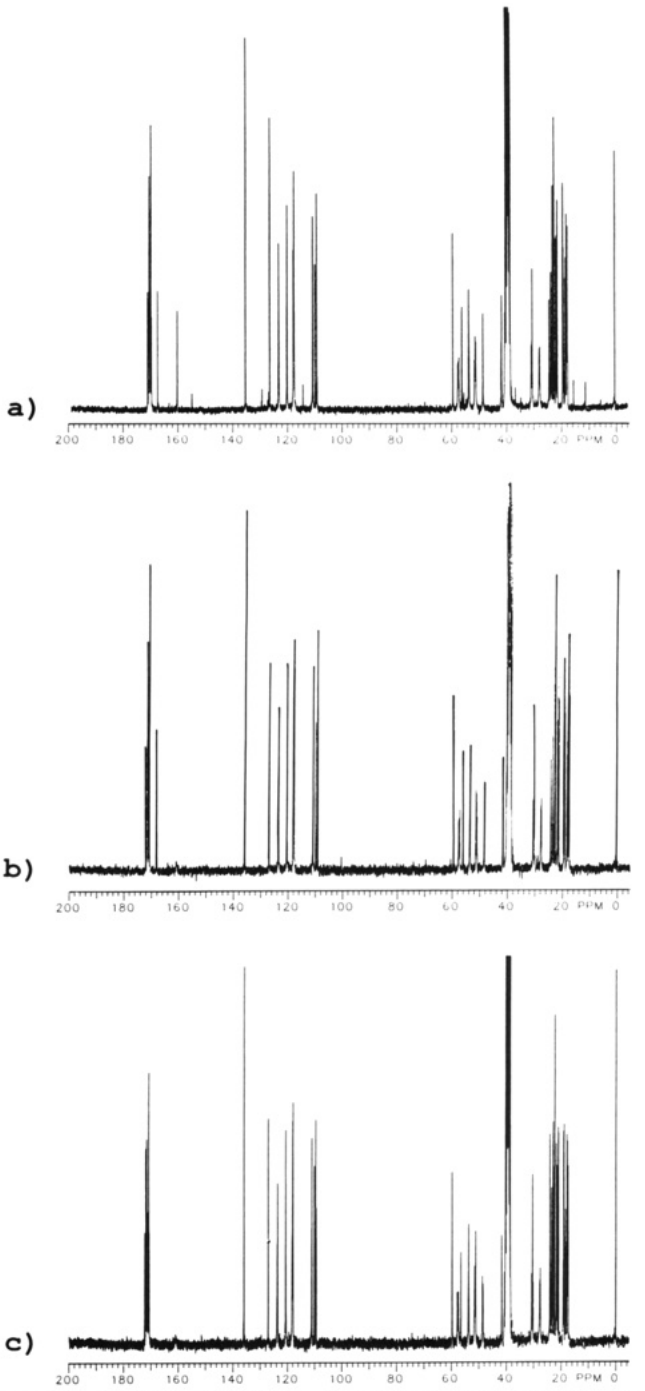

FIGURE 8: 75-MHz ^{13}C NMR spectra of (a) natural gramicidin at a concentration of 249 mg/mL (12000 scans), (b) ^{2}HCO-Val^1··· gramicidin A at a concentration of 91 mg/mL (16800 scans), and (c) ^{2}HCO-Val^1-D-Leu^2···gramicidin A at a concentration of 110 mg/mL (11500 scans). Samples are dissolved in ($^2H_6$) dimethyl sulfoxide with 1% tetramethylsilane. Spectra are recorded with a Varian XL300 spectrometer at room temperature with a deuterium lock and proton decoupling and are referenced to tetramethylsilane.

Figure 8 shows the ^{13}C NMR spectra of natural gramicidin and the synthetic products. Figure 8a is the ^{13}C NMR spectrum of natural gramicidin; the assignments of these resonances to specific carbon atoms have been made previously by others (Fossel et al., 1974; Prasad et al., 1982). Figure 8b is the ^{13}C NMR spectrum of ^{2}HCO-Val^1···gramicidin A, and this spectrum shows that ^{2}HCO-Val^1···gramicidin A possesses the same resonances as the Val^1···gramicidin A component of the natural mixture except for the resonance representing the carbonyl carbon of the formyl group which is absent in the synthetic product because of the directly bonded deuteron.

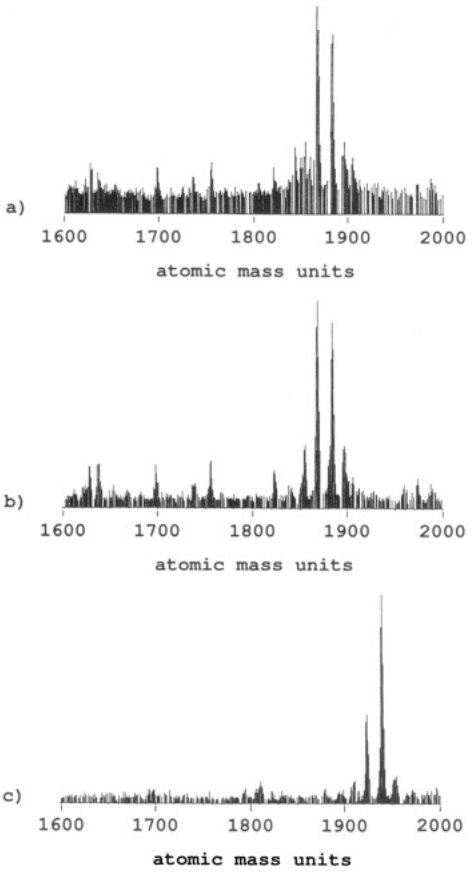

FIGURE 9: Mass spectra of (a) natural gramicidin, (b) ^{2}HCO-Val^1···gramicidin A, and (c) ^{2}HCO-Val^1-D-Leu^2···gramicidin A. Mass spectra of gramicidin are acquired with a VG ZAB-SE mass spectrometer by fast atom bombardment.

This spectrum helps confirm the identity of the product. Also, no major impurities are detected in the spectrum of Figure 8b. Figure 8c is the ^{13}C NMR spectrum of ^{2}HCO-Val^1-D-Leu^2···gramicidin A, and this spectrum shows that ^{2}HCO-Val^1-D-Leu^2···gramicidin A possesses the same resonances as the Val^1···gramicidin A component of the natural mixture except for the resonances representing the carbonyl carbon of glycine and the carbonyl carbon of the formyl group; these resonances are absent in the synthetic product because Gly^2 is replaced by D-Leu^2 and because the formyl group is deuterated. This spectrum helps confirm that the product is indeed ^{2}HCO-Val^1-D-Leu^2···gramicidin A. Also, no major impurities are observed in the spectrum of Figure 8c.

Mass spectra of natural gramicidin and the synthetic products are shown in Figure 9. The mass spectrum of natural gramicidin (Figure 9a) contains peaks centered about a peak of 1883 atomic mass units and peaks centered about a peak of 1867 atomic mass units. The peak at 1883 is consistent with the molecular weight of the Val^1···gramicidin A component of the natural mixture (1882), and a peak appearing 16 atomic mass units lower than the peak representing the molecular weight appears to be a characteristic feature of mass spectra of gramicidin obtained under these conditions. The mass spectrum of ^{2}HCO-Val^1···gramicidin A (Figure 9b) shows the same basic pattern as that of Val^1···gramicidin A except that one set of peaks is now centered about 1884, which is consistent with the 1883 molecular weight of ^{2}HCO-Val^1···gramicidin A. The mass spectrum of ^{2}HCO-Val^1-D-Leu^2···gramicidin A (Figure 9c) shows the same basic pattern as that of Val^1··· gramicidin A except that one set of peaks is now centered about 1940, which is consistent with the 1939 molecular weight of ^{2}HCO-Val^1-D-Leu^2···gramicidin A. These mass spectra therefore provide further confirmation of the identity of the synthetic products.

The amino acid analysis of the final products is displayed in Table III. Since the conditions under which the amino acid analysis is performed destroy tryptophan side chains, the tryptophan content of gramicidin cannot be assessed in this case. For the other amino acids, however, Table III shows that they are present in approximately the correct ratio for ^{2}HCO-Val^1···gramicidin A and for ^{2}HCO-Val^1-D-Leu^2··· gramicidin A.

ACKNOWLEDGMENTS

Thanks to Eric Kolodziej and Paul Toren for obtaining the mass spectra. Thanks to Jim Zobel for performing the amino acid analysis. Thanks to Dan Urry for providing the atomic coordinates of the left-handed, single-stranded, $\beta^{6.3}$ helical dimer. Thanks to Wan Lau for calculating the atomic coordinates of the various theoretical models of gramicidin structure.

REFERENCES

Adriaenssens, G. J., & Bjorkstam, J. L. (1972) *J. Chem. Phys. 56*, 1223–1225.

Arseniev, A. S., Bystrov, V. F., Ivanov, V. T., & Ovchinnikov, Y. A. (1984) *FEBS Lett. 165*, 51–56.

Arseniev, A. S., Barsukov, I. L., & Bystrov, V. F. (1985a) *FEBS Lett. 180*, 33–39.

Arseniev, A. S., Barsukov, I. L., Bystrov, V. F., Lomize, A. L., & Ovchinnikov, Y. A. (1985b) *FEBS Lett. 186*, 168–174.

Bamberg, E., & Läuger, P. (1973) *J. Membr. Biol. 11*, 177–194.

Bamberg, E., & Läuger, P. (1974) *Biochim. Biophys. Acta 367*, 127–133.

Beshah, K., Olejniczak, E. T., & Griffin, R. G. (1987) *J. Chem. Phys. 86*, 4730–4736.

Bradley, R. J., Prasad, K. U., & Urry, D. W. (1981) *Biochim. Biophys. Acta 649*, 281–285.

Busath, D., & Szabo, G. (1981) *Nature 294*, 371–373.

Bystrov, V. F., & Arseniev, A. S. (1988) *Tetrahedron 44*, 925–940.

Chapman, D., Urbina, J., & Keough, K. M. (1974) *J. Biol. Chem. 249*, 2512–2521.

Chapman, D., Cornell, B. A., Eliasz, A. W., & Perry, A. (1977) *J. Mol. Biol. 113*, 517–538.

Colonna-Cesari, F., Premilat, S., Heitz, F., Spach, G., & Lotz, B. (1977) *Macromolecules 10*, 1284–1288.

Datema, K. P., Pauls, K. P., & Bloom, M. (1986) *Biochemistry 25*, 3796–3803.

Flygare, W. H. (1964) *J. Chem. Phys. 41*, 206–214.

Fossel, E. T., Veatch, W. R., Ovchinnikov, Y. A., & Blout, E. R. (1974) *Biochemistry 13*, 5264–5275.

Glickson, J. D., Mayers, D. F., Settine, J. M., & Urry, D. W. (1972) *Biochemistry 11*, 477–486.

Heinemann, S. H., Stankovic, C. J., Delfino, J. M., Schreiber, S. L., & Sigworth, F. J. (1989) *Biophys. J. 55*, 505a.

Hing, A. W., Adams, S. P., Silbert, D. F., & Norberg, R. E. (1990) *Biochemistry* (preceding paper in this issue).

Hladky, S. B., & Haydon, D. A. (1970) *Nature 225*, 451–453.

Hladky, S. B., & Haydon, D. A. (1972) *Biochim. Biophys. Acta 274*, 294–312.

Ito, Y. (1986) *CRC Crit. Rev. Anal. Chem. 17*, 65–143.

Ito, Y., Sandlin, J., & Bowers, W. G. (1982) *J. Chromatogr. 244*, 247–258.

Kolb, H.-A., & Bamberg, E. (1977) *Biochim. Biophys. Acta 464*, 127–141.

Kolb, H.-A., Läuger, P., & Bamberg, E. (1975) *J. Membr. Biol. 20*, 133-154.
Kukolich, S. G. (1969) *J. Chem. Phys. 51*, 358-360.
Nicholson, L. K., Moll, F., Mixon, T. E., LoGrasso, P. V., Lay, J. C., & Cross, T. A. (1987) *Biochemistry 26*, 6621-6626.
Pauls, K. P., MacKay, A. L., Soderman, O., Bloom, M., Tanjea, A. K., & Hodges, R. S. (1985) *Eur. Biophys. J. 12*, 1-11.
Poupko, R., Luz, Z., Vega, A. J., & Zimmermann, H. (1987) *J. Chem. Phys. 86*, 5358-5364.
Prasad, B. V. V., & Chandrasekaran, R. (1977) *Int. J. Pept. Protein Res. 10*, 129-138.
Prasad, K. U., Trapane, T. L., Busath, D., Szabo, G., & Urry, D. W. (1982) *Int. J. Pept. Protein Res. 19*, 162-171.
Pschorn, O., & Spiess, H. W. (1980) *J. Magn. Reson. 39*, 217-228.
Sarges, R., & Witkop, B. (1965) *J. Am. Chem. Soc. 87*, 2027-2030.
Seelig, J. (1977) *Q. Rev. Biophys. 10*, 353-418.
Seelig, J. (1978) *Biochim. Biophys. Acta 515*, 105-140.
Seelig, J., Borle, F., & Cross, T. A. (1985) *Biochim. Biophys. Acta 814*, 195-198.
Spiess, H. W., & Sillescu, H. (1981) *J. Magn. Reson. 42*, 381-389.
Thadeus, P., Krishner, L. C., & Loubser, J. (1964) *J. Chem. Phys. 40*, 257-273.
Urry, D. W. (1971) *Proc. Natl. Acad. Sci. U.S.A. 68*, 672-676.
Urry, D. W., Goodall, M. C., Glickson, J. D., & Mayers, D. F. (1971) *Proc. Natl. Acad. Sci. U.S.A. 68*, 1907-1911.
Urry, D. W., Trapane, T. L., Romanowski, S., Bradley, R. J., & Prasad, K. U. (1983) *Int. J. Pept. Protein Res. 21*, 16-23.
Veatch, W. R., Fossel, E. T., & Blout, E. R. (1974) *Biochemistry 13*, 5249-5256.
Veatch, W. R., Mathies, R., Eisenberg, M., & Stryer, L. (1975) *J. Mol. Biol. 99*, 75-92.
Vega, A. J., & Luz, Z. (1987) *J. Chem. Phys. 86*, 1803-1813.
Venkatachalam, C. M., & Urry, D. W. (1983) *J. Comput. Chem. 4*, 461-469.
Wittebort, R. J., Olejniczak, E. T., & Griffin, R. G. (1987) *J. Chem. Phys. 86*, 5411-5420.
Zingsheim, H. P., & Neher, E. (1974) *Biophys. Chem. 2*, 197-207.

Resonance Raman Characterization of *Chromatium vinosum* Cytochrome *c'*. Effect of pH and Comparison of Equilibrium and Photolyzed Carbon Monoxide Species†

J. D. Hobbs,‡ R. W. Larsen,‡ T. E. Meyer,§ J. H. Hazzard,§ M. A. Cusanovich,§ and M. R. Ondrias*,‡

Department of Chemistry, University of New Mexico, Albuquerque, New Mexico 87131, and Department of Biochemistry, University of Arizona, Tucson, Arizona 85721

Received May 23, 1989; Revised Manuscript Received January 2, 1990

ABSTRACT: Resonance Raman spectra of *Chromatium vinosum* cytochrome *c'* have been obtained for the five pH-dependent states of the protein [i.e., types I (pH 7), II (pH 10), and III (pH 12) of the ferric protein and type a (pH 7) and type n (pH 12) of the ferrous protein]. The raman spectra of type II and type a are consistent with those of high-spin, 5-coordinate heme proteins, such as deoxyhemoglobin, while spectra of type III and type n correspond more closely to those of low-spin, ferric and ferrous cytochrome *c*, respectively. Spectra of the CO-bound equilibrium species qualitatively resemble those of carbon monoxy human HbA. However, both the Fe–C and C=O stretching modes of the ligated species exhibit pH-dependent frequency shifts. Our data also indicate that CO photolysis is much more efficient at pH 7 than at pH 12. Moreover, the spectra of the photolytic transients suggest that unique, high-spin species are formed subsequent to CO photolysis from both type a and type n species.

The bacterial cytochromes *c'* are a general class of mono- and diheme proteins found throughout photosynthetic and dentrifying bacteria (Bartsch, 1978; Meyer & Kamen, 1982). The cytochrome *c'* isolated from the purple photosynthetic bacterium *Chromatium vinosum* is a dimeric heme protein consisting of two identical subunits. Unlike most *c*-type heme proteins, ferrous cytochrome *c'* derived from *C. vinosum* reversibly binds carbon monoxide in its reduced form, but reacts with oxygen and nitric oxide irreversibly (Cusanovich, 1971; Kennel et al., 1972). The ferric form of this protein also binds cyanide (CN^-) and ethyl isocyanide with an affinity that is lower than that found for either horse heart cytochrome *c* or myoglobin (Kassner et al., 1985; Rubinow & Kassner, 1984).

The cytochromes *c'* exhibit several distinctive spectroscopic characteristics. In particular, the variations in their absorption spectra with pH have been of considerable interest. Ferric cytochromes *c'* exhibit three distinct types of UV-visible absorption and EPR spectra, depending upon the pH (Imai et al., 1969; Maltempo, 1975). In the UV-visible absorption, these have been labeled type I (pH 7), type II (pH 10), and

† This work was performed at the University of New Mexico and was supported by NIH Grants GM33330 (to M.R.O.) and GM21277 (to M.A.C.).
‡ University of New Mexico.
§ University of Arizona.

0006-2960/90/0429-4166$02.50/0